Physics Letters A 378 (2014) 723–727

Contents lists available at ScienceDirect

Physics Letters A

www.elsevier.com/locate/pla

Spaser spectroscopy with subwavelength spatial resolution

Yurii E. Lozovik [a,b,c,e,*], Igor A. Nechepurenko [b,d,e], Alexander V. Dorofeenko [b,d,e], Eugeny S. Andrianov [b,d,e], Alexander A. Pukhov [b,d,e]

[a] Institute of Spectroscopy RAS, Moscow Region, Troitsk, Russia
[b] Moscow Institute of Physics and Technology, Moscow Region, Dolgoprudny, Russia
[c] Moscow Institute of Electronics and Mathematics, HSE, Moscow, Russia
[d] Institute for Theoretical and Applied Electromagnetics RAS, Moscow, Russia
[e] All-Russia Research Institute of Automatics, Moscow, Russia

ARTICLE INFO

Article history:
Received 26 July 2013
Received in revised form 7 November 2013
Accepted 9 November 2013
Available online 10 January 2014
Communicated by V.M. Agranovich

Keywords:
Plasmonic nanolaser
Spaser
Microscopy
Intracavity spectroscopy

ABSTRACT

We propose a method for high-sensitivity subwavelength spectromicroscopy based on the usage of a spaser (plasmonic nanolaser) in the form of a scanning probe microscope tip. The high spatial resolution is defined by plasmon localization at the tip, as is the case for apertureless scanning near-field optical microscopy. In contrast to the latter method, we suggest using radiationless plasmon pumping with quantum dots instead of irradiation with an external laser beam. Due to absorption at the transition frequencies of neighboring nano-objects (molecules or clusters), dips appear in the plasmon generation spectrum. The highest sensitivity is achieved near the generation threshold.

1. Introduction

Recent developments in electrodynamics have largely been governed by a tendency to expand the range of applications of optical devices to fields where electronic, magnetic, X-ray, and other devices were conventionally used. Some examples include future optical computers [1,2], optical memory [3], optical lithography of high (subwavelength) spatial resolutions [4,5], and scanning near-field optical microscopy (SNOM) [6–15]. It is the use of the optical near field that makes it possible to overcome the Rayleigh limit of spatial resolution, $\sim \lambda$, which determines the lower bounds for the sizes of optical devices. The aperture realization of SNOM is based on light transmission through the small (subwavelength) hole. Since this is a tunneling process, it results in a small analyzed signal intensity and thus decreases sensitivity. This shortcoming can be overcome in apertureless schemes, including metal, where the incident electromagnetic wave is enhanced near a narrow needle tip of a scanning probe microscope (SPM) due to the "lighting rod effect" and resonance plasmon excitation at the tip. The greatest enhancement is achieved when the near-field excitations, surface plasmon polaritons (SPPs) [16], are excited at the tip. SPPs are capable of creating a relatively large field intensity in a small (subwavelength) spatial region [17], which is used in plasmonic lenses [18–22]. This property is also used in apertureless SNOM, where the near field (in the region near the tip of the SPM) created by the incident laser beam is scattered by an analyzed sample. This creates a signal in the far field, whose intensity (and in some schemes, phase) is measured and used for image retrieval. The apertureless SNOM method was also applied to second-harmonic imaging [23–27]. SNOM enables high-resolution images of the surface profile to be obtained, but the information about the sample composition is not provided by this method.

The latter limitation is overcome using tip-enhanced optical spectroscopy (TEOS), which exploits the principles of SNOM but analyzes the spectral response of the sample [28]. Thus, both the image and the composition of the sample are obtained. The most popular is the method based on Raman spectroscopy, tip-enhanced Raman spectroscopy (TERS) [29], which takes advantage of the large field intensity in SPPs.

However, the most sensitive spectral method is intracavity laser spectroscopy [30–32], which offers no spatial resolution but provides an extremely high sensitivity and reveals even forbidden (nondipolar) transitions [33]. This sensitivity is related to multiple passes (restricted by the cavity quality) of light through the sample. We believe that further development of spectroscopy should combine the TEOS and intracavity laser spectroscopy methods in order to combine their benefits.

In the current paper, we suggest a method of spectromicroscopy with ultrahigh spatial resolution and high sensitivity. These properties are inherited from the TEOS and laser spectroscopy methods,

* Tel.: +7 496 751 08 81.
E-mail address: lozovik@isan.troitsk.ru (Y.E. Lozovik).

0375-9601/$ – see front matter
http://dx.doi.org/10.1016/j.physleta.2013.11.044

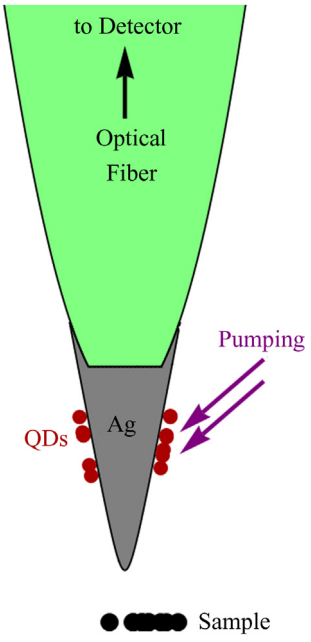

Fig. 1. Principal scheme of the tip-based spaser spectroscopy device (cross section). Quantum dots (QDs) are pumped by optical radiation and generate SPPs at the tip, which interacts with the sample. The signal, tunneled to the fiber, is detected.

although the proposed technique is very different from both of them and should lead to the appearance of a prospective class of methods for the study of nano-objects and surfaces. These methods use a spaser, a quantum plasmonic device which generates SPPs due to nonradiative energy transfer from the gain medium (a quantum dot) [34–37]. Although spasers require a high level of gain, recently, a few groups have reported on the realization of a spaser generating localized plasmons [38–40]. The generation of SPPs traveling along 1D and 2D structures is more straightforward, and corresponding spasers were realized by a number of groups [41–45]. The device suggested here is based on a 1D spaser generating SPPs traveling along a needle with a narrow tip. Due to the focusing property of the tip [46], the analyzed nano-object interacts effectively with the field of the plasmonic mode, concentrated near the needle tip [47–52], and can resonantly absorb the plasmon quanta. This process is analogous to the interaction with the field inside a laser cavity used in intracavity laser spectroscopy. The plasmonic lasing (spasing) can give a much higher field intensity than the TEOS scheme since the plasmon at the tip is excited not by the scattering of the incident wave but by direct nonradiative energy transfer from quantum dots or from another gain medium placed on the needle. The high field intensity favors high sensitivity. The advantage of the proposed method over standard laser spectroscopy, besides the high spatial resolution, is the weakness of the nanosized spaser compared to the macroscopic laser. In standard intracavity laser spectroscopy, the highest sensitivity is observed near (slightly above) the threshold [53], where the lasing becomes “weak”. In our case, the oscillation of the nanosized laser is easily suppressed by absorption in the analyzed sample, which gives outstanding sensitivity.

2. Free spaser spectrum

A principal scheme of the spaser spectroscope is shown in Fig. 1. The needle geometry typical of near-field devices supports a plasmonic solution. One may use a tapered dielectric optical fiber with narrow metallic tip. A mode propagating along the needle is localized between the needle tip and the metal/dielectric fiber interface. Thus, a cavity is formed for a plasmonic mode, which is

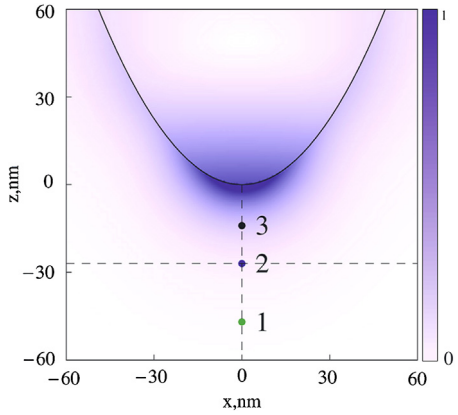

Fig. 2. The electric field intensity distribution near the tip. The crossing of the dashed lines (point 2) denotes the point of the optimum sample position.

amplified by a set of quantum dots deposited onto the needle or by any other gain medium; a 1D spaser is formed. One can use optical pumping at a frequency higher than that of quantum dots. The luminescence leads to the radiation at the quantum dot transition frequency, which presents a possibility to filter out the noise. Then the energy is radiated at the quantum dot transition frequency in the optical range. The field enhanced by the tip (Fig. 2) interacts effectively with the analyzed sample. The field’s localization ensures spatial resolution of the order of the tip’s curvature radius. Signal detection may be performed by a spectral analysis of light, scattered by the system, in the same way as it is done using the TEOS technique. Alternatively, the wave, having tunneled to the optical fiber, may be transferred to a spectral analyzer. In principle, the device can also be realized as a long metal needle with Bragg corrugation [54,55], which localizes the plasmonic mode at the needle tip.

In the classical methods of laser spectroscopy [30–32], the spectral line of the analyzed sample is scanned by tuning the frequency of the laser with very narrow line or by using a multimode laser [33]. In the scheme based on the spaser, the line width is increased by a few orders of magnitude due to strong noise in the metal. Indeed, since the cavity mode has a lifetime shorter than the transverse relaxation time, T_2, of the quantum dots, the spasing line width is mostly determined by T_2^{-1}. The absorption peaks of the sample molecules are often narrower than the spasing line. Such a situation is not characteristic of traditional narrow-line lasers, although it is known in the linear case, where Rabi splitting leads to the appearance of a dip in a cavity spectral line [56]. In the nonlinear case, it is not obvious whether a narrow absorption peak suppresses the whole spasing or creates a dip in the spectral line. It is shown below that each spectral line of the sample is displayed as a dip in the homogeneously broadened spectral line of the spaser. Further, inhomogeneous broadening due to the variation of transition frequencies of different quantum dots can broaden the spectral line up to that of SPPs. Therefore, the device suggested here has no tunable elements in its simplest realization. Below, we analyze the results of homogeneous broadening only and neglect nonlocal effects [57–59], which are substantially exhibited in smaller-scale plasmonic structures (smaller than several nanometers) [58,59] and in some specific (e.g., epsilon-near-zero) metamaterials [57,60]. Recently, the spasing spectra were calculated near [61] and above the threshold [62].

In most papers devoted to traditional laser spectroscopy, one reasonably neglects quantum noise effects [33], except when working near the threshold [53]. The ordinary situation is a set of dense and narrow cavity modes, some of which are suppressed by absorption in the sample particles. Alternatively, one uses a single-mode laser with a very narrow spectral line. Then the absorption

spectrum is scanned by tuning the cavity frequency. In all these cases, consideration of the quantum noise is generally of no use. In our case, we use an approximation of single-mode plasmonic lasing (spasing), which is homogeneously broadened by noise in a metallic needle. First, the single-mode approximation is justified by the possibility of selecting a plasmonic mode of the needle. Although a metallic paraboloid has a set of plasmonic solutions with different dispersion relations, $\omega_i(k)$, $i = 0, 1, 2, \ldots$, the frequency, ω, is specified by the transition of quantum dots, and the wave number is determined by the distance between the needle tip and the metal/dielectric interface (see Fig. 1). Second, the consideration of broadening is necessary because the sample spectrum is observed within the spaser's spectral line. Its width is completely due to noise. According to the fluctuation–dissipation theorem, the noise source is also the source of dissipation in metal.

The spaser dynamics are described by Maxwell–Bloch equations, which follow from the Maxwell equations and from the equations for the density matrix of the gain medium atoms. These are partial differential equations that are reduced to ordinary differential equations by using the single-mode approximation [63], which represents the electric field as a product of a (dimensionless) time amplitude and a cavity mode, $\mathbf{E}(\mathbf{r})$. In our case, the latter is the field distribution in the plasmonic mode of the needle. Further simplification of the equations is attained by using the approximation of slow varying amplitude, which reduces the second-order equations to first-order ones. This gives a system of equations for the amplitude of the cavity mode, a, polarization of the gain medium, σ, and population inversion, D [64]:

$$\dot{a} = -a/\tau_a - i\Omega\sigma + F(t), \tag{1a}$$

$$\dot{\sigma} = (i\delta - 1/T_2)\sigma + i\Omega a D, \tag{1b}$$

$$\dot{D} = -(D - D_0)/T_1 + 2i\Omega\left(a^*\sigma - \sigma^* a\right). \tag{1c}$$

These equations show that the population inversion is pushed toward the value of D_0 by pumping and is simultaneously suppressed by the field. At positive values of D, oscillations of σ and a are produced; as a result, spasing appears.

The system's behavior is modeled at realistic parameters. The longitudinal and transverse relaxation times are $T_1 \sim 10^{-13}$ s and $T_2 \sim 10^{-13}$ s for CdSe quantum dots. It is known that ~30 CdSe quantum dots per 1 μm of length are enough for spasing [35]. In the present paper, we consider a system of 100 quantum dots. For the tip curvature radius, $\rho \cong 20$ nm, the cavity mode (plasmon) relaxation time can be evaluated based on the absorption losses in the metal. Thus, $\tau_a = (2\int(\partial(\varepsilon'\omega)/\partial\omega)\mathbf{E}\mathbf{E}^* dV)/(\omega\int\varepsilon''\mathbf{E}\mathbf{E}^* dV) \sim 10^{-14}$ s. Here, the plasmon field distribution, $\mathbf{E}(\mathbf{r})$, is assessed for the infinite cylinder of permittivity characteristic of silver at $\lambda = 350$ nm [65]. For a larger ρ, the radiation losses should be taken into account [45,66]. For the smaller values of the tip curvature radius, $\rho < 5$ nm, correction associated with the electron hole pairs ($\omega_0\tau_a \sim \rho/r_{\mathrm{TF}}$, r_{TF} is the Thomas–Fermi screening radius) [52] should also be taken into account. The interaction constant is given as $\Omega = \sqrt{\mu\omega/8\hbar W}$, where the mode energy is $W = (8\pi)^{-1}\int(\partial(\varepsilon'\omega)/\partial\omega)\mathbf{E}\mathbf{E}^* dV$, and the constant μ [63] is given by $\mu \cong |\mathbf{d}_{12}|^2\langle\mathbf{E}^2\rangle_\Sigma$ (the subscript Σ denotes the average over the metal surface, where the quantum dots are located) and the transition dipole moment of a QD is estimated as $|\mathbf{d}_{12}| \cong 20D$. This gives the evaluation $\Omega \sim 10^{12}$–10^{13} s^{-1}. Detuning $\delta = \omega_a - \omega_0$ of the cavity frequency from the gain medium transition frequency is taken to be zero.

Without taking into account the noise, $F(t)$, the stationary lasing spectrum, would be a Dirac delta function. The simplest approach to the spectrum calculation is a direct solution of the Langevin-type equation system (1) using the delta-correlated (white) noise, $\langle F(t)F(t+\tau)\rangle = 2\delta(\tau)/\tau_a$, where the angle brackets correspond to an average over the random process realizations,

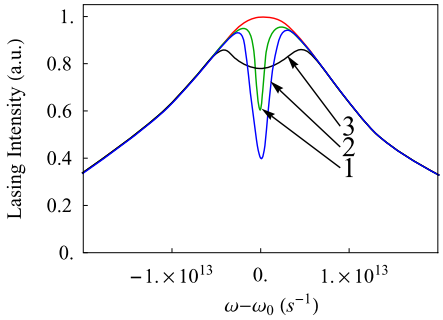

Fig. 3. The lasing spectrum of the spaser (unnumbered line) and its change caused by interaction with the sample (the curve numbers correspond to points in Fig. 2).

and the factor $2/\tau_a$ follows from the analysis of the system's interaction with the reservoir. This interaction leads to both cavity mode dissipation and fluctuations [67]. The direct calculation of the spectrum of the stochastic signal, $a(t)$, is challenging because the signal is unbounded in time. On the other hand, the autocorrelator, $C(t) = \langle a^*(0)a(t)\rangle$, decays exponentially when time goes to infinity [68]. Therefore, a convenient way to approach the lasing spectrum calculation is to use the Wiener–Khinchin theorem, $S(\omega) = (2\pi)^{-1}\int_{-\infty}^{\infty} C(t)\exp(i\omega t)\,dt$. This result is shown by the unnumbered line in Fig. 3. Note that the current approach takes into account not only the phase diffusion but also amplitude fluctuations, which are strong in the noisy plasmonic lasers, especially near the lasing threshold.

3. Spectrum modification by the sample molecule

Interaction of the plasmonic laser with nano-objects, which resonantly absorb plasmon quanta in some narrow spectral range, leads to the appearance of a dip in the spasing spectrum. The absorbing nano-objects are described by equations similar to (1b) and (1c) with negative pumping. Such an approach takes absorber saturation effects into account. Thus, the system (1) assumes the following form:

$$\begin{aligned}
&\dot{a} = -a/\tau_a - i\Omega\sigma - i\Omega_S\sigma_S + F(t),\\
&\dot{\sigma} = (i\delta - 1/T_2)\sigma + i\Omega a D,\\
&\dot{D} = -(D - D_0)/T_1 + 2i\Omega\left(a^*\sigma - \sigma^* a\right),\\
&\dot{\sigma}_S = (i\delta_S - 1/T_{2S})\sigma_S + i\Omega_S a D_S,\\
&\dot{D}_S = -(D_S - D_{0S})/T_{1S} + 2i\Omega_S\left(a^*\sigma_S - \sigma_S^* a\right).
\end{aligned} \tag{2}$$

The subscript S denotes the variables related to the analyzed sample. The value of D_{0S} is proportional to the number of sample absorbing particles (atoms, molecules, etc.), $D_{0S} = N\tilde{D}_{0S}$. The value of $\tilde{D}_{0S}$ is the difference between the populations of the top and bottom levels for a single particle and should be negative to describe absorption rather than gain, $-1 \leqslant \tilde{D}_{0S} < 0$. In our calculations, we assume that in the absence of a field, the particles are at their ground state (i.e., $\tilde{D}_{0S} = -1$). The longitudinal and transverse relaxation times for the sample particles may vary over a wide range; we have used the values $T_{1S} \sim 4\cdot 10^{-12}$ s and $T_{2S} \sim 4\cdot 10^{-12}$ s. The effect of the sample, positioned near the tip, is determined by its overlap with the plasmon field so that the interaction constant between the spaser and sample is $\Omega_S = \sqrt{\mu_S\omega/8\hbar W}$, where $\mu_S \sim |\mathbf{d}_{12S}|^2\langle\mathbf{E}^2\rangle_S$ and $\langle\cdots\rangle_S$ denote an average over the sample. The field distribution (Fig. 2) was calculated for the parabolic form of the tip. Since its curvature radius, $\rho \sim 20$ nm, is far below the wavelength, the field was found with the electrostatic approximation using parabolic coordinates. In fact, the value of Ω_S is tuned by a vertical shift of the needle (Fig. 4a) and may be considered to be a free parameter.

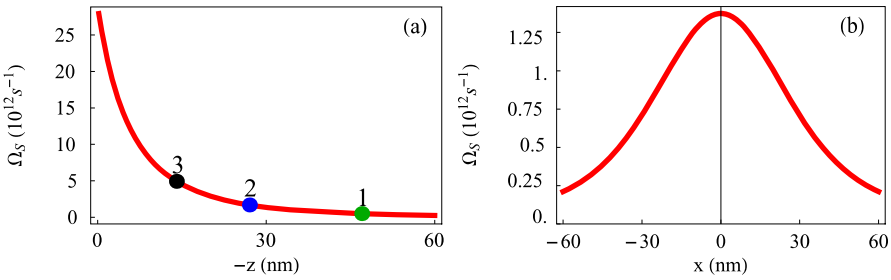

Fig. 4. Interaction constant of the spaser with an analyzed object as a function of (a) vertical and (b) horizontal coordinates of the sample ($D_0 = -20$, see the text). The point numbers correspond to those in Fig. 2. The sample particles have dipole moments typical of atomic transition, $d_{12S} = 1D = 10^{-18}$, CGS units.

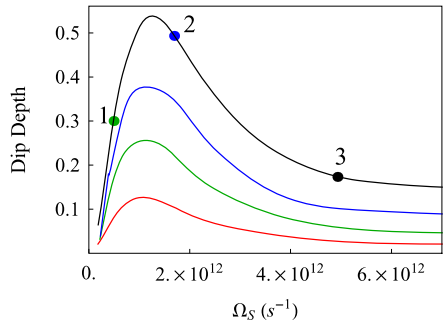

Fig. 5. Dependence of the spectral dip depth on the interaction constant, Ω_S (i.e., on the vertical position of the needle). The numbers correspond to those in Figs. 2–4. The curves (from the bottom to the top) correspond to 5, 10, 15, and 20 sample atoms, respectively.

The numerical solution of the equation system (2) gives the spasing spectrum when the Wiener–Khinchin theorem is applied. For a weak interaction (where the needle is far from the sample [i.e., at small values of Ω_S]), the dip in the generation spectrum is also weak (curve 1 in Fig. 3). Growth of the interaction increases the dip (curve 2 in Fig. 3) but finally broadens it (curve 3 in Fig. 3), which leads to a decrease in its depth and of the spectral resolution. Thus, an optimal needle position exists, which can be found from the maximal value of the dip in the generation spectra (Fig. 5). Alternatively, one may use the "quality factor" of the dip. Fig. 5 shows that a cluster as small as a dozen atoms creates a considerable dip in the spasing spectrum, so the method demonstrates good sensitivity.

The spatial resolution can be estimated from the spatial dependence of the interaction constant, which is shown in Fig. 4b. It is seen that the spot around the optimal point, where the interaction constant is substantial, is of the order of the tip curvature radius (20 nm). The influence of the atoms appearing to the side of the optimum point may be estimated from Fig. 5 since the value of Ω_S describes the interaction irrespective of the sample's shift direction. Thus, the following curious feature appears: if the tip is too close to the analyzed surface, then the region, which creates the best resolved spectrum (similar to curve 2 in Fig. 3), forms a circle. Inside this circle, a "broadened-spectrum region" is located, where the spectrum is similar to that shown by the curve 3 in Fig. 3, whereas the outside region weakly interacts (the spectrum is similar to that shown by curve 1 in Fig. 3). Presumably, such a response may cause confusion, and it is better to place the tip at the optimal or at a slightly farther distance from the sample.

Note that the possibility of the detection of tiny quantities of a substance follows from the nanoscopic size of the spaser. Indeed, to create a dip in the spaser spectrum, the absorbing particles should suppress oscillations at their transition frequency. Of course, such suppression is much easier in the case of a spaser than in the case of a traditional (macroscopic) laser, which is responsible for the high sensitivity of spaser spectroscopy.

It should be also noted that in the present paper, the spasing line broadening was modeled through the noise in metal. Another possible mechanism exists — namely, the inhomogeneous broadening of the gain medium transition line, which is due to the variation of the quantum dot size. However, near the threshold, where the spaser spectroscope is most sensitive, the first approach gives an incorrect value of sensitivity. This value diverges when the pumping tends to the threshold value, and accounting for noise is required to restrict the sensitivity [53]. Therefore, accounting for homogeneous broadening is necessary in our analysis, and accounting for inhomogeneous broadening will be performed elsewhere.

4. Conclusion

In conclusion, in this paper, a method of scanning spaser spectromicroscopy is suggested. It combines the benefits of tip-enhanced optical spectroscopy and intracavity laser spectroscopy. The use of a nanolaser (spaser) as a source of plasmons in the TEOS scheme increases the field intensity. On the one hand, in comparison with traditional laser spectroscopy, a nanosized spaser is damped down easily by only a few dozen of sample atoms. On the other hand, the spaser has a broad spectral line due to losses, and narrow absorption lines of the sample appear as a set of dips in the spectrum. Instead of scanning over the sample spectrum, one can observe the absorption lines as dips in the spasing line.

Acknowledgements

The authors would like to thank professors Alexey Vinogradov and Ilya Ryzhikov for useful discussions. This work is partly supported by RFBR grants (12-02-01093-a, 13-02-00407-a, 13-08-01062-a, 13-02-92660, 14-02-00850) and by the Dynasty Foundation. Y.E.L. was supported by Program of Basic Research of HSE.

References

[1] H.J. Caulfield, S. Dolev, Why future supercomputing requires optics, Nat. Photonics 4 (5) (2010) 261–263.
[2] R.S. Tucker, The role of optics in computing, Nat. Photonics 4 (7) (2010) 405.
[3] D. Pile, Optical memory: Rephasing stored light, Nat. Photonics 5 (12) (2011) 712.
[4] N. Fang, et al., Sub-diffraction-limited optical imaging with a silver superlens, Science 308 (5721) (2005) 534–537.
[5] M.M. Alkaisi, et al., Sub-diffraction-limited patterning using evanescent near-field optical lithography, Appl. Phys. Lett. 75 (22) (1999) 3560–3562.
[6] E.A. Ash, G. Nicholls, Super-resolution aperture scanning microscope, Nature 237 (5357) (1972) 510–512.
[7] R. Bachelot, P. Gleyzes, A.C. Boccara, Reflection-mode scanning near-field optical microscopy using an apertureless metallic tip, Appl. Opt. 36 (10) (1997) 2160–2170.
[8] A.A. Budini, Open quantum system approach to single-molecule spectroscopy, Phys. Rev. A 79 (4) (2009) 043804.
[9] J.-B. Decombe, et al., Living cell imaging by far-field fibered interference scanning optical microscopy, Opt. Express 19 (3) (2011) 2702–2710.

[10] R. Esteban, R. Vogelgesang, K. Kern, Full simulations of the apertureless scanning near field optical microscopy signal: achievable resolution and contrast, Opt. Express 17 (4) (2009) 2518–2529.
[11] Y. Inouye, S. Kawata, Near-field scanning optical microscope with a metallic probe tip, Opt. Lett. 19 (3) (1994) 159–161.
[12] D.W. Pohl, W. Denk, M. Lanz, Optical stethoscopy: Image recording with resolution λ_{20}, Appl. Phys. Lett. 44 (7) (1984) 651–653.
[13] T. Taubner, R. Hillenbrand, F. Keilmann, Performance of visible and mid-infrared scattering-type near-field optical microscopes, J. Microsc. 210 (3) (2003) 311–314.
[14] F. Zenhausern, Y. Martin, H.K. Wickramasinghe, Scanning interferometric apertureless microscopy: optical imaging at 10 angstrom resolution, Science 269 (5227) (1995) 1083–1085.
[15] V.V. Klimov, M. Ducloy, V.S. Letokhov, A model of an apertureless scanning microscope with a prolate nanospheroid as a tip and an excited molecule as an object, Chem. Phys. Lett. 358 (3–4) (2002) 192–198.
[16] S.I. Bozhevolniy (Ed.), Plasmonic Nanoguides and Circuits, Pan Stanford Publishing, Singapore, 2009.
[17] S.I. Bozhevolnyi, I.I. Smolyaninov, A.V. Zayats, Near-field microscopy of surface-plasmon polaritons: Localization and internal interface imaging, Phys. Rev. B 51 (24) (1995) 17916–17924.
[18] J.B. Pendry, Negative refraction makes a perfect lens, Phys. Rev. Lett. 85 (18) (2000) 3966–3969.
[19] I.I. Smolyaninov, Y.-J. Hung, C.C. Davis, Magnifying superlens in the visible frequency range, Science 315 (5819) (2007) 1699–1701.
[20] I.I. Smolyaninov, et al., Far-field optical microscopy with a nanometer-scale resolution based on the in-plane image magnification by surface plasmon polaritons, Phys. Rev. Lett. 94 (5) (2005) 057401.
[21] P.A. Belov, et al., Transmission of images with subwavelength resolution to distances of several wavelengths in the microwave range, Phys. Rev. B 77 (19) (2008) 193108.
[22] P.A. Belov, C.R. Simovski, P. Ikonen, Canalization of subwavelength images by electromagnetic crystals, Phys. Rev. B 71 (19) (2005) 193105.
[23] W. Dickson, et al., Near-field second-harmonic imaging of thin ferromagnetic films, Appl. Phys. Lett. 85 (26) (2004) 6341–6343.
[24] Z.-Y. Li, B.-Y. Gu, G.-Z. Yang, Strong localization of near-field second-harmonic generation for nonlinear mesoscopic surface structures, Phys. Rev. B 59 (19) (1999) 12622–12626.
[25] S. Takahashi, A.V. Zayats, Near-field second-harmonic generation at a metal tip apex, Appl. Phys. Lett. 80 (19) (2002) 3479–3481.
[26] A. Zayats, Apertureless near-field microscopy of second-harmonic generation, in: S. Kawata, V.M. Shalaev (Eds.), Tip Enhancement, Elsevier, 2011, p. 235.
[27] A.V. Zayats, V. Sandoghdar, Apertureless scanning near-field second-harmonic microscopy, Opt. Commun. 178 (1–3) (2000) 245–249.
[28] A. Hartschuh, Tip-enhanced optical spectroscopy, Philos. Trans. R. Soc., Math. Phys. Eng. Sci. 362 (1817) (2004) 807–819.
[29] B. Pettinger, Single-molecule surface- and tip-enhanced Raman spectroscopy, Mol. Phys. 108 (16) (2010) 2039–2059.
[30] S. Stenholm, Foundations of Laser Spectroscopy, John Wiley & Sons, New York, 1987.
[31] W. Demtröder, Laser Spectroscopy. Basic Concepts and Instrumentation, Springer, Berlin, 2002.
[32] H. Abramczyk, Introduction to Laser Spectroscopy, Elsevier, Amsterdam, 2005.
[33] V.M. Baev, T. Latz, P.E. Toschek, Laser intracavity absorption spectroscopy, Appl. Phys. B, Lasers Opt. 69 (3) (1999) 171–202.
[34] D.J. Bergman, M.I. Stockman, Surface plasmon amplification by stimulated emission of radiation: Quantum generation of coherent surface plasmons in nanosystems, Phys. Rev. Lett. 90 (2003) 027402.
[35] A.A. Lisyansky, et al., Channel spaser: Coherent excitation of one-dimensional plasmons from quantum dots located along a linear channel, Phys. Rev. B 84 (15) (2011) 153409.
[36] D.E. Chang, et al., Quantum optics with surface plasmons, Phys. Rev. Lett. 97 (5) (2006) 053002.
[37] D.Y. Fedyanin, A.V. Arsenin, Surface plasmon polariton amplification in metal–semiconductor structures, Opt. Express 19 (13) (2011) 12524–12531.
[38] M.A. Noginov, et al., Demonstration of a spaser-based nanolaser, Nature 460 (7259) (2009) 1110–1112.
[39] S. Xiao, et al., Loss-free and active optical negative-index metamaterials, Nature 466 (7307) (2010) 735–738.
[40] J.Y. Suh, et al., Plasmonic bowtie nanolaser arrays, Nano Lett. 12 (11) (2012) 5769–5774.
[41] R.F. Oulton, et al., Plasmon lasers at deep subwavelength scale, Nature 461 (7264) (2009) 629–632.
[42] M.T. Hill, et al., Lasing in metal–insulator–metal sub-wavelength plasmonic waveguides, Opt. Express 17 (13) (2009) 11107–11112.
[43] R.A. Flynn, et al., A room-temperature semiconductor spaser operating near 1.5 μm, Opt. Express 19 (9) (2011) 8954–8961.
[44] O. Hess, K.L. Tsakmakidis, Metamaterials with quantum gain, Science 339 (6120) (2013) 654–655.
[45] V. Klimov, Nanoplasmonics, Pan Stanford Publishing, 2013.
[46] M.I. Stockman, Nanofocusing of optical energy in tapered plasmonic waveguides, Phys. Rev. Lett. 93 (13) (2004) 137404.
[47] Y.E. Lozovik, S.P. Merkulova, The outlook for nanolocal femtosecond spectroscopy and nanolithography, Phys. Usp. 42 (3) (1999) 284–285.
[48] Y.E. Lozovik, A.V. Klyuchnik, S.P. Merkulova, Nanolocal optical study and nanolithography using scanning probe microscope, Laser Phys. 9 (2) (1999) 552–556.
[49] A.J. Babadjanyan, N.L. Margaryan, K.V. Nerkararyan, Superfocusing of surface polaritons in the conical structure, J. Appl. Phys. 87 (8) (2000) 3785–3788.
[50] A. Normatov, et al., Efficient coupling and field enhancement for the nanoscale: plasmonic needle, Opt. Express 18 (13) (2010) 14079–14086.
[51] S. Berweger, et al., Light on the tip of a needle: plasmonic nanofocusing for spectroscopy on the nanoscale, J. Phys. Chem. Lett. 3 (7) (2012) 945–952.
[52] Y.E. Lozovik, A.V. Klyuchnik, The dielectric function and collective oscillations inhomogeneous systems, in: L.V. Keldysh, D.A. Kirzhnits, A.A. Maradudin (Eds.), Dielectric Susceptibility, North Holland, Amsterdam, 1987, p. 299.
[53] H. Kimble, Calculated enhancement for intracavity spectroscopy with a single-mode laser, IEEE J. Quantum Electron. 16 (4) (1980) 455–461.
[54] V.S. Volkov, S.I. Bozhevolnyi, Nanophotonic components utilizing channel plasmon polaritons, in: S.I. Bozhevolniy (Ed.), Plasmonic Nanoguides and Circuits, Pan Stanford Publishing, Singapore, 2009, p. 317.
[55] Y. Gong, J. VuCkovic, Design of plasmon cavities for solid-state cavity quantum electrodynamics applications, Appl. Phys. Lett. 90 (3) (2007), 033113-3.
[56] Y. Zhu, et al., Vacuum Rabi splitting as a feature of linear-dispersion theory: Analysis and experimental observations, Phys. Rev. Lett. 64 (21) (1990) 2499–2502.
[57] G.A. Wurtz, et al., Designed ultrafast optical nonlinearity in a plasmonic nanorod metamaterial enhanced by nonlocality, Nat. Nanotechnol. 6 (2) (2011) 107–111.
[58] F.J. García de Abajo, Nonlocal effects in the plasmons of strongly interacting nanoparticles, dimers, and waveguides, J. Phys. Chem. C 112 (46) (2008) 17983–17987.
[59] J.M. McMahon, S.K. Gray, G.C. Schatz, Nonlocal optical response of metal nanostructures with arbitrary shape, Phys. Rev. Lett. 103 (9) (2009) 097403.
[60] R.J. Pollard, et al., Optical nonlocalities and additional waves in epsilon-near-zero metamaterials, Phys. Rev. Lett. 102 (12) (2009) 127405.
[61] E.S. Andrianov, et al., Spectrum of surface plasmons excited by spontaneous quantum dot transitions, J. Exp. Theor. Phys. 117 (2) (2013) 205–213.
[62] P. Ginzburg, A.V. Zayats, Linewidth enhancement in spasers and plasmonic nanolasers, Opt. Express 21 (2) (2013) 2147–2153.
[63] A.E. Siegman, Lasers, University Science Books, Mill Valley, CA, 1986.
[64] H. Haken, Laser Theory, Springer-Verlag, Berlin, 1984.
[65] E.D. Palik, Handbook of Optical Constants of Solids, Academic Press, San Diego, 1998.
[66] D. Martín-Cano, et al., Resonance energy transfer and superradiance mediated by plasmonic nanowaveguides, Nano Lett. 10 (8) (2010) 3129–3134.
[67] R. Pantell, H. Puthoff, Fundamentals of Quantum Electronics, Wiley, New York, 1969.
[68] H. Risken, The Fokker-Planck-Equation. Methods of Solution and Applications, Springer-Verlag, Berlin, 1989.